

Article

Linker-Free Magnetite-Decorated Gold Nanoparticles (Fe₃O₄-Au): Synthesis, Characterization, and Application for Electrochemical Detection of Arsenic (III)

Mohammed Sedki ^{1,†}, Guo Zhao ^{2,†,‡}, Shengcun Ma ³, David Jassby ³ and Ashok Mulchandani ^{2,4,*} 

¹ Materials Science and Engineering Program, University of California, Riverside, CA 92521, USA; mabue002@ucr.edu

² Department of Chemical and Environmental Engineering, University of California, Riverside, CA 92521, USA; zhaoguo@njau.edu.cn

³ Department of Civil and Environmental Engineering, University of California, Los Angeles, CA 90095, USA; shengcun@ucla.edu (S.M.); jassby@ucla.edu (D.J.)

⁴ Center for Environmental Research and Technology (CE-CERT), University of California, Riverside, CA 92507, USA

* Correspondence: adani@engr.ucr.edu

† These authors contributed equally to this work.

‡ Current address: College of Artificial Intelligence, Nanjing Agricultural University, Nanjing 210031, China.

Abstract: Linker-free magnetite nanoparticles (Fe₃O₄NPs)-decorated gold nanoparticles (AuNPs) were grown using a new protocol that can be used as a new platform for synthesis of other intact metal-metal oxide nanocomposites without the need for linkers. This minimizes the distance between the metal and metal oxide nanoparticles and ensures the optimum combined effects between the two material interfaces. X-ray diffraction (XRD) and Fourier transform infrared (FTIR) spectroscopy confirmed the successful synthesis of the Fe₃O₄-Au nanocomposite, without any change in the magnetite phase. Characterization, using transmission electron microscopy (TEM), scanning electron microscopy (SEM) and energy dispersive X-ray (EDX) spectroscopy, revealed the composite to consist of AuNPs of 70 ± 10 nm diameter decorated with tiny 10 ± 3 nm diameter Fe₃O₄NPs in Au:Fe mass ratio of 5:1. The prepared Fe₃O₄-Au nanocomposite was embedded in ionic liquid (IL) and applied for the modification of glassy carbon electrode (GCE) for the electrochemical detection of As(III) in water. By combining the excellent catalytic properties of the AuNPs with the high adsorption capacity of the tiny Fe₃O₄NPs towards As(III), as well as the good conductivity of IL, the Fe₃O₄-Au-IL nanocomposite showed excellent performance in the square wave anodic stripping voltammetry detection of As(III). Under the optimized conditions, a linear range of 1 to 100 µg/L was achieved with a detection limit of 0.22 µg/L (S/N = 3), and no interference from 100-fold higher concentrations of a wide variety of cations and anions found in water. A very low residual standard deviation of 1.16% confirmed the high precision/reproducibility of As(III) analysis and the reliability of the Fe₃O₄-Au-IL sensing interface. Finally, this proposed sensing interface was successfully applied to analyzing synthetic river and wastewater samples with a 95–101% recovery, demonstrating excellent accuracy, even in complex synthetic river and wastewater samples containing high concentrations of humic acid without any sample pretreatments.

Keywords: arsenic detection; linker-free; gold-magnetic nanoparticles; square wave anodic stripping voltammetry; ionic liquid



Citation: Sedki, M.; Zhao, G.; Ma, S.; Jassby, D.; Mulchandani, A. Linker-Free Magnetite-Decorated Gold Nanoparticles (Fe₃O₄-Au): Synthesis, Characterization, and Application for Electrochemical Detection of Arsenic (III). *Sensors* **2021**, *21*, 883. <https://doi.org/10.3390/s21030883>

Academic Editor: Ki-Hyun Kim
Received: 24 December 2020
Accepted: 25 January 2021
Published: 28 January 2021

Publisher's Note: MDPI stays neutral with regard to jurisdictional claims in published maps and institutional affiliations.



Copyright: © 2021 by the authors. Licensee MDPI, Basel, Switzerland. This article is an open access article distributed under the terms and conditions of the Creative Commons Attribution (CC BY) license (<https://creativecommons.org/licenses/by/4.0/>).

1. Introduction

The contamination of arsenic in water is a significant concern to human health [1–3], as exposure can lead to a range of acute and chronic diseases, such as dysphasia, facial edema, dehydration, jaundice, and cancer [4–10]. Inorganic arsenic compounds, arsenite (As(III)) and arsenate (As(V)) commonly exist in the environment either due to geochemical

enrichment or industrial processes. Arsenite and arsenate are more toxic than the organic forms. Arsenite, which is the most toxic, is a mobile and soluble form of arsenic [11]. Usually, the content of As(III) in water is a serious problem, because even though its concentration is very low, it is highly toxic even at trace levels and can enter the human body in different ways, causing serious health problems. The World Health Organization (WHO) has recommended an upper limit of 10 ppb for total arsenic in drinking water [11].

Different analytical strategies based on spectrometry, such as atomic fluorescence spectrometry [12], inductively coupled plasma mass spectrometry (ICP-MS) [13] and graphite furnace atomic absorption spectrometry [14] are frequently used to determine As(III) at trace levels in a variety of samples. While these techniques have high sensitivity for As(III) detection, they have limitations of high operating cost, expensive instruments, requirement of professional operators and bulky instrumentation, which make them unsuitable for on-site routine analysis.

In contrast to these methods, electrochemical analyses, and in particular, anodic stripping voltammetry (ASV), is a low cost, low limit of detection (LOD) sensing method that has the benefit of convenient operation, high sensitivity, and the ability to perform real-time analysis [15,16]. Usually, the fabrication of an electrochemical sensor based on electrode modification can be divided into the following steps [15–18]: 1. nanocomposites synthesis and characterization; 2. electrode fabrication and pretreatment; 3. electrode modification using the synthesized nanocomposites. Electrodes of various nano-materials/particles, such as carbon nanotubes, metal oxides, noble metals (Au, Ag and Pt), and graphene, have been used for As(III) determination [15–18]. Previous reports demonstrated that AuNPs-modified electrodes could enhance the anodic current response toward As(III) more effectively than other materials relying on chemical reduction by electrogenerated H₂ [19–25]. However, these methods need strong acidic conditions to guarantee enough electrogenerated H₂ availability for electrochemical reduction of As(III) to As(0) during the electrochemical reduction/deposition step. This limits the application of Au-based materials for the detection of As(III) by non-professionals and in the field.

Recently, a number of Fe₃O₄-based materials have been synthesized for arsenic removal because of the excellent arsenic adsorption ability of Fe₃O₄ [26,27]. In addition, some studies have been performed utilizing Fe₃O₄-based materials to analyze the concentration of As(III) [28,29]. However, the poor conductivity of Fe₃O₄ has limited its sensitivity for electrochemical detection. To improve the electrode conductivity and electrocatalytic activity, electrodes modified with Au-Fe₃O₄ nanocomposite were reported [30,31]. However, the synthesis procedures used linkers such as oleic acid, oleyl amine, or aminopropyl trimethoxy silane to attach/decorate Au nanoparticles on Fe₃O₄, required a high temperature and high-pressure autoclave for Fe₃O₄ synthesis, and were time-consuming (~24 h). The linker introduces separation between the adsorbed As(III) on magnetite and the Au nanoparticle catalyst that could potentially reduce electron transfer rate/efficiency [32]. Moreover, a large fraction of the adsorbing material surface area was covered/blocked by Au NPs.

Here, we report linker-free grown AuNPs decorated with Fe₃O₄NPs (Fe₃O₄-Au) nanocomposite using a facile, faster and green chemistry synthesis route for application in chemically modified electrode ASV detection of As (III) in water. The important differences in the nanocomposite material between this work and the literature include the morphology/architecture and synthesis method as follows. (1) There is no linker between Fe₃O₄ and Au, which minimizes the distance between the metal and metal oxide nanoparticles and ensures the optimum combined effects between the two material interfaces. (2) Nanocomposite consists of AuNPs (70 nm average diameter) decorated with very tiny (10 nm average diameter) Fe₃O₄NPs which provide a higher surface area of the adsorbent for As(III). (3) The synthesis uses a co-precipitation method that is performed at low temperature (80 °C) and atmospheric pressure and does not require harsh organic solvents to synthesize Fe₃O₄NPs.

The introduced material was used to modify the surface of a glassy carbon electrode ($\text{Fe}_3\text{O}_4\text{-Au-IL/GCE}$) and applied as a working electrode in the ASV detection of As(III). The results exhibited a comparable or higher sensitivity than the modified electrodes reported in the literature. The combination of AuNPs, Fe_3O_4 NPs, and IL resulted in many intriguing combined effects and catalytic abilities, such as an excellent ability to adsorb As(III), high electrical conductivity and good stability. In addition, the synthesis method introduced in this work can be used as a new platform for synthesis of intact metal- Fe_3O_4 nanocomposites without the need for any linkers to achieve the optimum combined effects between the materials. Moreover, the electrode materials were characterized using different techniques (CV, SEM, EDS, XRD, TEM and EIS). Furthermore, a dual-catalysis system has been proposed for the first time to investigate and explain the catalytic mechanism behind the phenomenon. Finally, the analytical application of $\text{Fe}_3\text{O}_4\text{-Au-IL/GCE}$ was tested for the measurement of As(III) in synthetic river water and wastewater samples.

2. Experimental

2.1. Reagents and Instruments

Ferrous chloride ($\text{FeCl}_2 \cdot 4\text{H}_2\text{O}$), ferric chloride ($\text{FeCl}_3 \cdot 6\text{H}_2\text{O}$), ethylene glycol (EG), ammonium hydroxide (NH_4OH , 25%), sodium citrate, sodium hydroxide (NaOH), hydrogen tetrachloroaurate ($\text{HAuCl}_4 \cdot 3\text{H}_2\text{O}$), polyvinyl alcohol (PVA), sodium acetate (CH_3COONa), ammonium acetate ($\text{CH}_3\text{COONH}_4$), monopotassium phosphate (KH_2PO_4), sodium bicarbonate (NaHCO_3), manganese sulfate (MnSO_4), zinc sulfate (ZnSO_4), magnesium sulfate (MgSO_4), and calcium chloride (CaCl_2) were purchased from Fisher Scientific (USA). Humic acid sodium salt (Technical grade) was purchased from Sigma-Aldrich. Ionic liquid ($[\text{C}_4\text{dmim}][\text{NTf}_2]$) was obtained from IoLiTec Ionic Liquids Technologies, INC. (USA). Arsenic trioxide (As_2O_3) was purchased from Strem Chemicals, INC. (USA). An As(III) stock solution (1 mg/mL) was prepared by dissolving As_2O_3 in the 1.0 M aqueous NaOH. Sodium acetate trihydrate was obtained from Fisher Scientific (USA) and prepared as acetate buffer solution (0.2 M) with acetic acid for the electroanalysis of As(III).

The prepared Fe_3O_4 NPs (magnetite), AuNPs, and $\text{Fe}_3\text{O}_4\text{-Au}$ were characterized by scanning electron microscopy (SEM, Zeiss 1540 XB Crossbeam scanning electron microscope.), transmission electron microscopy (TEM, FEI Tecnai12), energy dispersive X-ray spectroscopy (EDX), X-ray diffraction (XRD, PANalytical Empyrean Series 2), and Fourier transform infra-red (FTIR, Thermo Nicolet 6700) spectroscopy. Electrochemical analysis, i.e., cyclic voltammetry (CV), square wave anodic stripping voltammetry (SWASV), and electrochemical impedance spectroscopy (EIS) were performed on a CH Instrument 760C electrochemical workstation. A three-electrode system and a 20 mL cell were used for all measurements, in which $\text{Fe}_3\text{O}_4\text{-Au-IL/GCE}$, Pt wire, and Ag/AgCl electrode were used as working, counter, and reference electrodes, respectively. During the deposition step, the test solution was stirred using a magnetic stir bar. The As(III) in synthetic wastewater detected by ICP-MS (PerkinElmer NexION 2000) was used to confirm the robustness of our synthesis method in complex water streams.

2.2. Synthesis and Modification of $\text{Fe}_3\text{O}_4\text{-Au-IL}$ Nanocomposite

In this procedure, Fe_3O_4 NPs were prepared using the co-precipitation method, as reported earlier [33], with some modifications. The de-ionized (DI) water and reagents used in this procedure were all de-oxygenated before use. In brief, a mixture of $\text{FeCl}_2 \cdot 4\text{H}_2\text{O}$ and $\text{FeCl}_3 \cdot 6\text{H}_2\text{O}$ (20 mg and 32 mg, respectively) was added to the solution consisting of 20 mL of DI water and 20 mL of EG. The mixed solution was heated to 60 °C with stirring under nitrogen purging. Ammonia solution (5%) was added dropwise to the above solution until reaching the pH of 10, and then the reaction mixture was agitated for half an hour. The obtained mixture was washed a few times with DI water by means of an external magnet to remove the excess ammonia solution and surfactant. Quantities of 10 mL of $\text{HAuCl}_4 \cdot 3\text{H}_2\text{O}$ (20 mg/mL) and 10 mL of EG were added to the obtained Fe_3O_4 NPs and stirred for 2 min at 80 °C. Then, 5 mL of sodium citrate (0.3%) was added to the $\text{Fe}_3\text{O}_4\text{-Au}^{3+}$ solution and

stirred at 80 °C for half an hour to obtain the Fe₃O₄-Au nanocomposite. The prepared suspension was washed with DI water by means of an external magnet to remove the excess surfactants and the free AuNPs that were not bonded to magnetite, if any. A quantity of 4 mL of Fe₃O₄-Au nanocomposite solution (1 mg/mL) was mixed with 300 µL of 0.5% ionic liquid (IL) in ethanol to obtain the Fe₃O₄-Au-IL hybrid structure. The surface of GCE was polished by 0.05 µm alumina powder before modification, and was then immersed in 1:1 HNO₃, absolute ethanol and water for sonication, separately. Subsequently, 8 µL of the Fe₃O₄-Au-IL suspension was drop-casted onto the surface of GCE and dried in oven at 60 °C. Other electrodes were prepared the same way as described above.

2.3. Stripping Voltammetry Analysis of As(III)

The electrochemical measurements of SWASV were performed in a 0.2 M acetate buffer solution (pH 5.0) containing different concentrations of As(III). Unless stated otherwise, −0.9 V was used as a deposition/reduction potential for the pre-deposition of As(III) under stirring for 200 s. The stirring was stopped once the deposition step was completed. An anodic stripping voltammogram was obtained from −0.4 to 0.3 V after an equilibration period of 10 s. The frequency, amplitude and potential step were 25 Hz, 25 mV and 5 mV, respectively. To regenerate the modified electrode before the next measurement at the end of stripping, an oxidation potential of 0.6 V was applied to the working electrode for 120 s to remove any As(0) residuals which may not be completely stripped from the electrode surface.

2.4. Preparation of Water Samples

DI water containing 150 ppm magnesium nitrate, 60 ppm ammonia chloride, 500 ppm calcium chloride, 50 ppm sodium citrate and 500 ppm potassium calcium chloride (1260 ppm total dissolved solids), simulating the chemical composition of Yamuna River in Northern India, was spiked with As(III) and tested with the developed sensor to evaluate sensor performance. To further validate the robustness of our electrode, the electrode was used to measure As(III) in synthetic wastewater, the recipe of which was modified from the literature [34] and listed in Table S1. In these experiments, a 10 mL water sample test solution composed of 9 mL simulated water and 1 mL 2 M acetate buffer (pH 5.0) was used for each measurement to ensure the pH 5.0 buffer condition with 0.2 M acetate.

3. Results and Discussion

In this work, we employ the concept of adsorbent-assisted stripping voltammetry analysis for sensitive detection of As(III) based on a sensing interface of AuNPs decorated with Fe₃O₄NPs (Fe₃O₄-Au). AuNPs have excellent catalytic properties and the Fe₃O₄NPs are highly adsorptive to As(III), which makes Fe₃O₄-Au a very promising material for the stripping voltammetry analysis of As(III). Additionally, ionic liquids (IL) have high adhesiveness, conductivity, work across a wide potential window, and have been widely used in the modification of electrodes [35–40]. Incorporating IL into the nanocomposite should further enhance the sensitivity and stability of the sensing interface on the electrode surface.

The synthesis method introduced in this work can be used as a new platform for synthesis of intact metal-Fe₃O₄ nanocomposites without the need for any linkers, which minimizes the distance between the metal and metal oxide nanoparticles and ensures the optimum combined effects between the materials. In this method, EG could provide magnetite with hydroxyl groups that facilitate the chelation of Au³⁺ ions (Fe₃O₄-Au³⁺), as illustrated in the schematic diagram of Figure 1. In this novel platform method, sodium citrate is a mild reducing and capping agent that can reduce gold ions slowly into AuNPs [41,42], while it will not reduce Fe^{3+/2+} in magnetite and hence it enables the synthesis of the Fe₃O₄-Au nanocomposite in situ without any linkers.

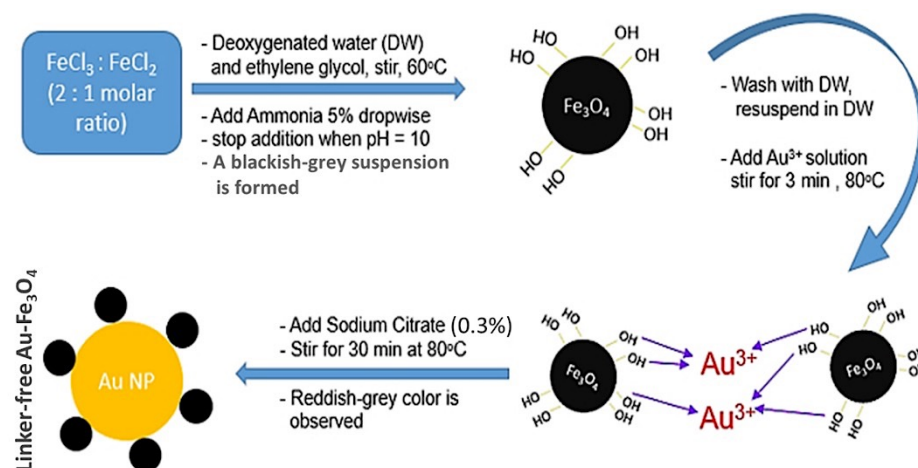


Figure 1. Schematic of Fe₃O₄-Au nanoparticle preparation and the suggested mechanism of its formation.

3.1. Physicochemical Characterization of Fe₃O₄-Au Nanocomposite

The introduced synthesis method is time saving (1–2 h), as the synthesis of magnetite NPs was conducted using the co-precipitation method. It is also linker-free with no barrier between gold and magnetite, which improves the electron transfer between them and enhances their combined effects. This procedure uses simple chemicals that are mostly ecofriendly, and very easy to wash using deionized water, if any excess is present. In addition, magnetite nanoparticles were prepared to be very tiny (≈ 10 nm) to allow for higher surface area and higher adsorption of As(III). The morphology and sizes of the prepared particles were assessed using SEM and TEM imaging as illustrated in Figure 2. The synthesized Fe₃O₄-Au suspension was drop-casted as a thin film on a piece of silicon wafer, at the same concentration and volume used in preparing the electrode materials, and sputtered with Pd/Pt to reduce surface charging, and then imaged by SEM. The SEM image in Figure 2a illustrates that AuNPs (the bigger and brighter particles) are surrounded by much smaller Fe₃O₄NPs. However, the Fe₃O₄NPs were not well resolved. Further imaging of Fe₃O₄-Au by TEM (Figure 2b) shows a 70 nm spherical core AuNP decorated with Fe₃O₄NPs, which agrees with the SEM image. The TEM image of Fe₃O₄NPs showed the particles are spherical with an average size of 10 ± 3 nm (Figure 2c,d). The TEM images confirm the success of the proposed platform, as the AuNPs and Fe₃O₄NPs are directly bound to each other without separation between them. Furthermore, EDX spectroscopy was implemented to calculate the actual weight ratio between Au and Fe in the prepared nanocomposite. The results in Supplementary Figure S1, determined that the weight ratio is approximately 5:1 (Au:Fe).

The results of the XRD analysis of magnetite (Fe₃O₄) NPs in Figure 3 show diffraction peaks at 30.17° , 35.53° , 43.27° , 56.96° , 62.69° , which can be assigned to the (220), (311), (400), (511), and (440) planes of the cubic inverse spinel-type structure of magnetite (PDF#85-1436) [43,44]. Moreover, the diffraction pattern of Fe₃O₄-Au has the same peaks of magnetite addressed above in addition to the characteristic peaks of the face-centered cubic (FCC) AuNPs at 38.23° , 44.54° , 64.71° , 77.69° , which can be assigned to the (111), (200), (220), and (311) planes, (Pattern 4-784) [45]. Hence, the XRD data confirm the successful synthesis of the Fe₃O₄-Au nanocomposite, without any change in the magnetite phase. Moreover, the intensity of AuNPs peaks is higher because they are in a higher concentration, which agrees with the EDS data, in which the weight ratio is around 5:1 (Au:Fe) (Figure S1). FTIR spectrum analysis (Figure 4) of Fe₃O₄NPs shows a broad peak centering at 3380 cm^{-1} and two peaks at 2900 and 2915 cm^{-1} , which are attributed to the stretching vibrations of O-H and C-H groups from EG, respectively. In addition, Fe-O vibrations show two peaks at 1380 and 565 cm^{-1} . Vibrational peaks of Fe₃O₄NPs are in a good agreement with published work [46]. On the other hand, the spectrum of AuNPs shows stretching

vibrations of O-H groups of PVA at 3320 cm^{-1} , vibrations of C=O groups of sodium citrate at 1730 cm^{-1} and stretching vibrations of C-H groups at 2900 and 2915 cm^{-1} . The FTIR spectrum of $\text{Fe}_3\text{O}_4\text{-Au}$ contains all the peaks from both spectra of Au and Fe_3O_4 , which confirms the successful synthesis of this nanocomposite.

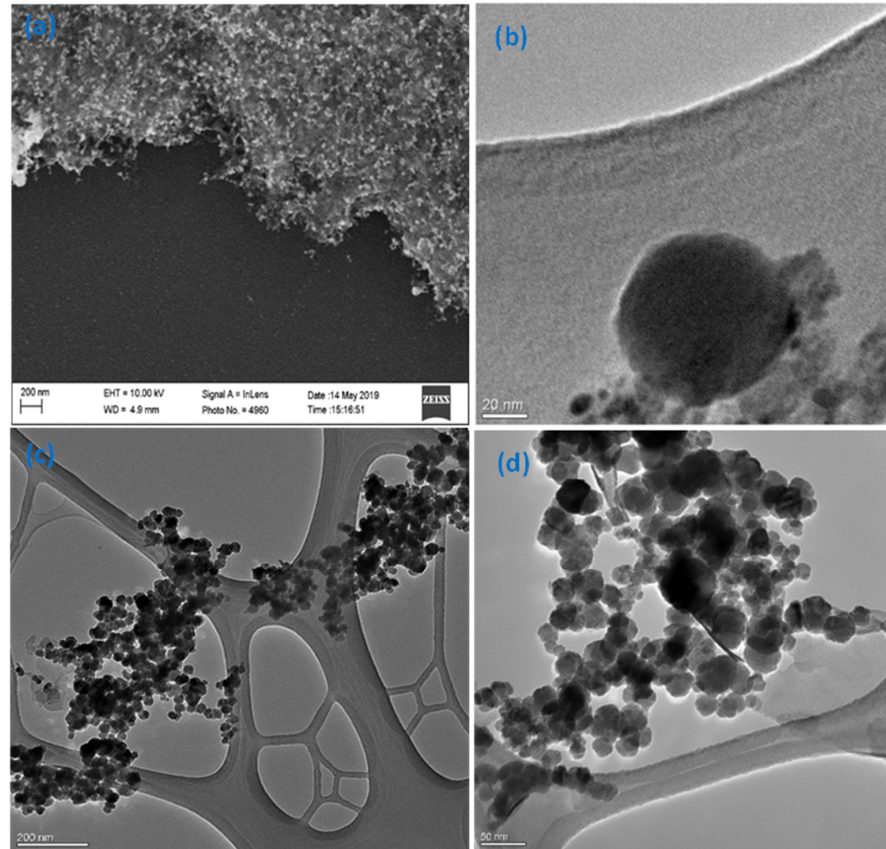


Figure 2. Electron microscopy images. (a) SEM image of a thin film of $\text{Fe}_3\text{O}_4\text{-Au}$ nanocomposite on a silicon wafer sputtered with Pd/Pt, (b) a higher resolution TEM image of the prepared nanocomposite, and (c,d) TEM images of the Fe_3O_4 NPs.

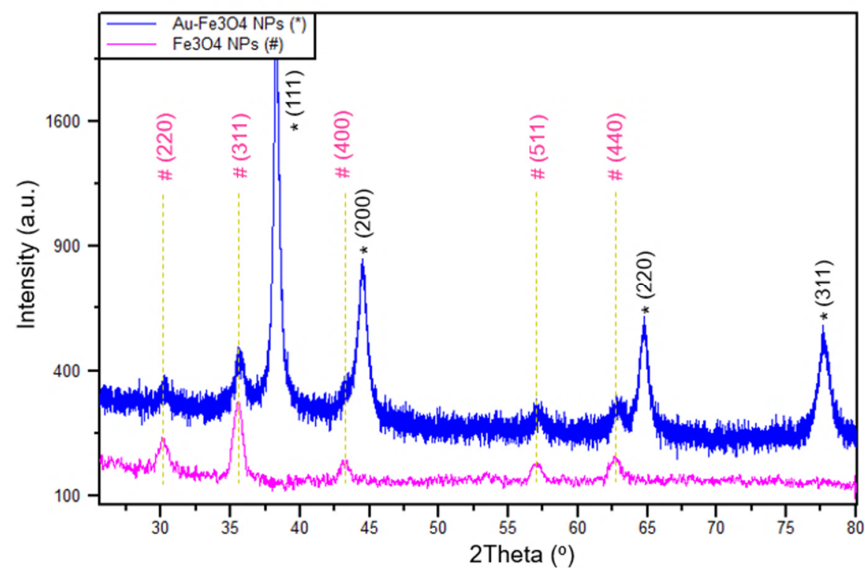


Figure 3. XRD patterns of Fe_3O_4 NPs and $\text{Fe}_3\text{O}_4\text{-Au}$.

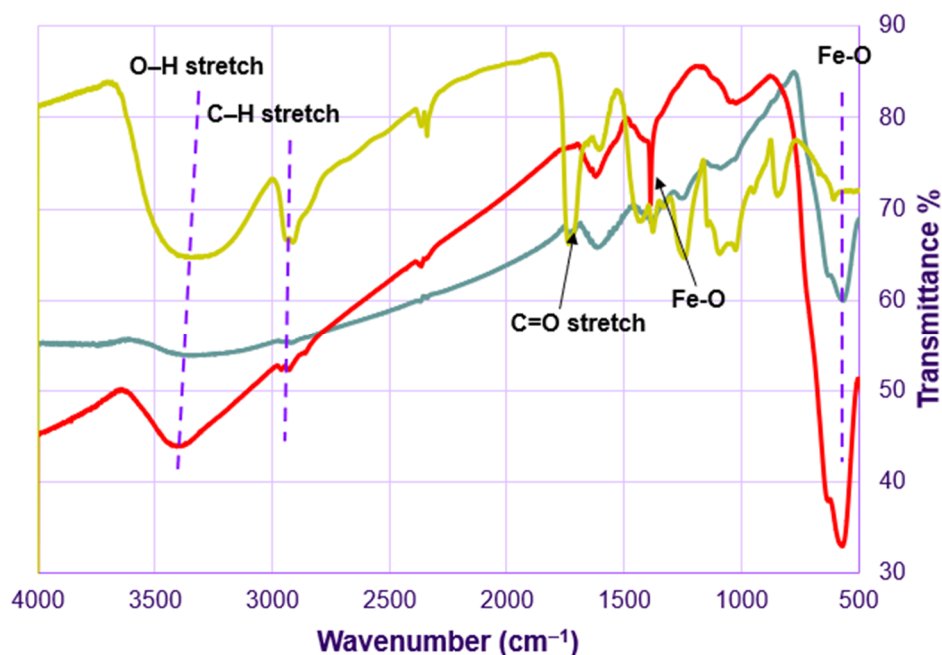


Figure 4. FTIR spectra of Fe₃O₄ (red), Au (yellow), and Fe₃O₄-Au (blue).

3.2. Electrochemical Characterizations of Modified Electrodes

The electrochemical characteristics of bare GCE and different modified GCEs, i.e., Fe₃O₄NPs/GCE, Fe₃O₄-Au/GCE, and Fe₃O₄-Au-IL/GCE were investigated using CV based on a ferri/ferrocyanide [Fe(CN)₆]^{3−/4−} redox probe (Figure S2A). On the bare GCE, two well-defined redox peaks of [Fe(CN)₆]^{3−/4−} were found in curve a. When compared to the bare GCE, Fe₃O₄NPs/GCE showed a decreased redox current of [Fe(CN)₆]^{3−/4−}, because of the poor conductivity of Fe₃O₄. However, stronger redox peaks were found with the Fe₃O₄-Au/GCE (curve c) compared to the Fe₃O₄NPs/GCE, due to the excellent electrical conductivity of the AuNPs. Furthermore, the addition of IL to the nanocomposite, i.e., Fe₃O₄-Au-IL/GCE, increased its conductivity and resulted in stronger redox peaks.

EIS was used to explore the material/electrode interface properties and changes based on the impedance changes (Figure S2B). The EIS results show different semicircles, each with a diameter equivalent to the charge transfer resistance (R_{ct}), which corresponds to the process of electron transfer limitation [47–49]. Based on the value of semicircle diameter, the order of the R_{ct} of different modified electrodes was as follows: Fe₃O₄/GCE (curve b) > Fe₃O₄-Au/GCE (curve c) > Fe₃O₄-Au-IL/GCE > bare GCE (curve a). The EIS results are consistent with those of CV.

3.3. Optimization of Analysis Parameters

Deposition potential and deposition time play a key role in the SWASV sensitivity (stripping peak current/concentration) of heavy metals detection. Additionally, Fe₃O₄NPs and AuNPs play a unique role in the dual-catalytic system for the SWASV detection of As(III). Therefore, in this study, responses of Fe₃O₄-Au-IL/GCE toward As(III) were investigated to find optimal values of deposition potential, deposition time and the mass ratio of Fe₃O₄ to AuNPs. Figure 5A shows the influence of deposition potential on the stripping peak current of 20 ppb As(III) for 200 s deposition time and Fe: Au of 1:5. As shown in the figure, the stripping peak current increased with an increase of deposition potential reaching a maximum at −0.9 V followed by a small decrease at deposition potential above −0.9 V. The lower currents at potentials below −0.9 V are ascribed to incomplete reduction of As(III). On the other hand, the small decrease in current at deposition potentials above −0.9 V are the result of hydrogen evolution. Thus, the deposition potential of −0.9 V was chosen for As(III) preconcentration.

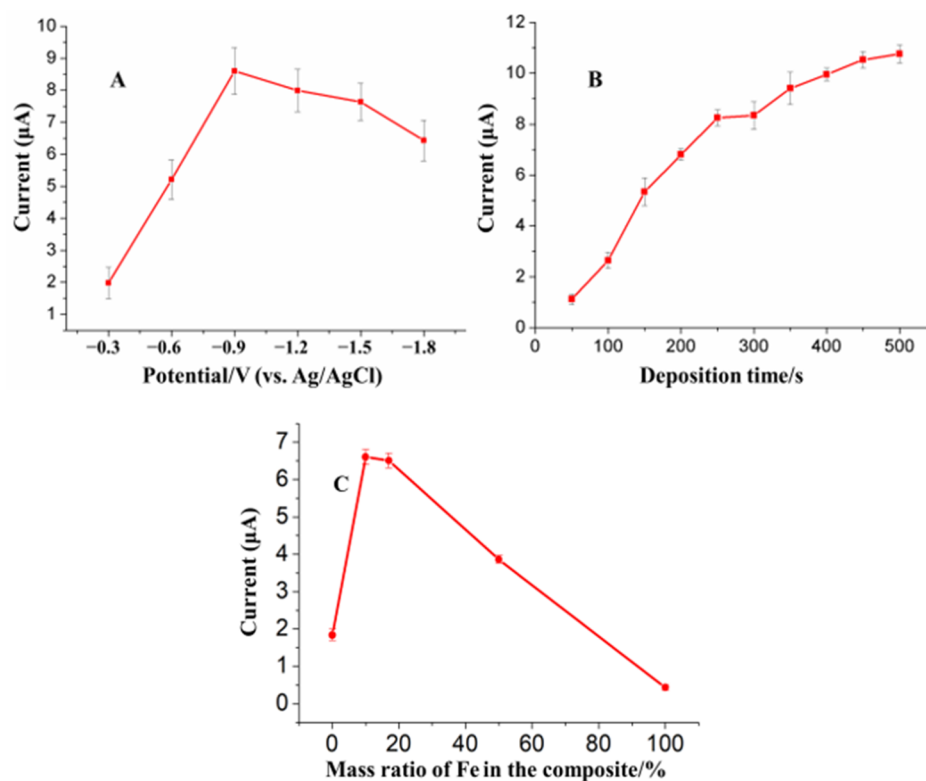


Figure 5. (A) Effect of the deposition potential, (B) deposition time and (C) weight ratio between Fe and Au on stripping current for 20 ppb (A,B) and 50 ppb (C) of As(III) in 0.2 M pH 5.5 acetate buffer at Fe_3O_4 -Au-IL/GCE. Each data point is an average of 5 measurements from 3 electrodes and error bars represent ± 1 standard deviation.

The effect of deposition time on the peak current of 20 ppb As(III) at -0.9 V deposition potential and Fe:Au of 1:5 is shown in the Figure 5B. The results show a monotonic increase in peak current as a function of deposition time. The direct relation between the current and deposition time suggests a lower LOD could be expected by increasing the deposition time. However, as a longer deposition time implies a longer analysis time, we selected a 200 s deposition period.

Different mass ratios of AuNPs to Fe_3O_4 NPs in Fe_3O_4 -Au composite on the stripping peak current of 50 ppb As(III) at -0.9 V deposition potential and 200 s deposition time were examined (Figure 5C). The results show an increase in the stripping peak current from 1.8 μA to ~ 6.6 μA when the Fe_3O_4 -Au composite contained 10 to 16.3% (by mass) of Fe followed by a rapid drop to ~ 0.3 μA for 100% Fe (i.e., Fe_3O_4 NPs only). This indicates a clear complementarity relationship between the two components of the nanocomposite in enhancing the sensitivity of the sensor for As(III) detection. It is interesting that although Fe_3O_4 NPs have a strong adsorption capacity for the As(III), the response on Fe_3O_4 NPs/GCE was the smallest. That may be ascribed to the poor conductivity of Fe_3O_4 NPs, which affects both reduction of As(III) to As(0) and the oxidation of As(0) to As(III) on the electrode surface. Additionally, while the stripping response on AuNPs/GCE was higher than Fe_3O_4 NPs/GCE, it was lower than Fe_3O_4 -Au/GCE at different Fe mass ratios. This may be attributed to the combined effect of the strong adsorption capacity of Fe_3O_4 and good conductivity and catalytic ability of AuNPs. Based on cost and maximum sensitivity, Fe_3O_4 -Au nanocomposite containing 16.3% (by mass) Fe was selected as the optimum composition.

3.4. Analytical Characteristics of Fe_3O_4 -Au-IL/GCE for As(III)

The stripping responses of 50 $\mu\text{g/L}$ As(III) on bare GCE and different modified electrodes are shown in Figure 6. As shown in Figure 6A, almost no stripping response was obtained on the bare GCE. The stripping response of As(III) on Fe_3O_4 NPs/GCE was not significant either, due to the poor conductivity of Fe_3O_4 NPs. In contrast, at the Fe_3O_4 -Au/GCE, a higher stripping peak signal was obtained due to the combined effect of Fe_3O_4 NPs and AuNPs, which can be ascribed to the dual-catalysis system (Figure 6B). H_2 was electrogenerated on the AuNP decorated with Fe_3O_4 NPs at the applied negative potential during the electrodeposition step. The generated H_2 then donates electrons in the reduction of As(III) to As(0), and forms H^+ ions. Due to the strong adsorption capacity of Fe_3O_4 NPs, As(III) concentration near the electrode surface gradually increased, which enhanced the catalytic efficiency of H_2 on the As(III) adsorbed to Fe_3O_4 NPs even at a high pH condition (the first catalytic system). Furthermore, the surface-activated Fe(II) can also donate an electron to form Fe(III), which helps reduce As(III). The produced Fe(III) will then acquire an electron, to revert to Fe(II), from either the electrode or the oxidation of As(0) to As(III) during the stripping process of SWASV. The procedure described above is a complete Fe(II)/Fe(III) cycle. During this process, the electron transfer between electrode and As(III) was mediated by Fe(II), which was used as an electrocatalyst (the second catalytic system). This mediation of the Fe(II)/Fe(III) cycle together with the catalysis of AuNPs will efficiently promote the deposition of As(III) and further enhance the sensitivity toward the electrochemical detection of As(III) [23,50]. Additionally, the stripping peak current was further improved with Fe_3O_4 -Au-IL/GCE due to the good conductivity and adhesiveness of IL.

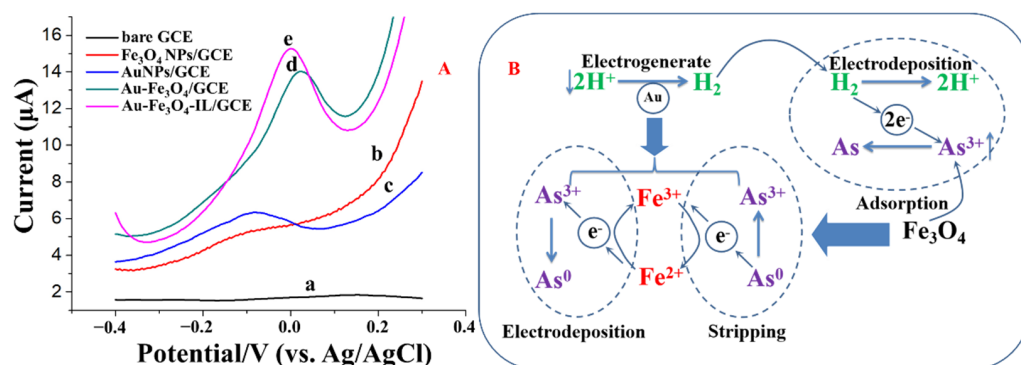


Figure 6. (A) The SWASV responses of 50 $\mu\text{g/L}$ As(III) on different modified electrodes; (a) bare GCE, (b) Fe_3O_4 NPs/GCE, (c) AuNPs/GCE, (d) Fe_3O_4 -Au/GCE and (e) Fe_3O_4 -Au-IL/GCE. (B) The catalytic mechanism of Fe_3O_4 -Au in the electroanalysis of As(III). Glassy carbon electrode (GCE); ionic liquid (IL).

3.4.1. Sensitivity, Limit of Detection, and Reproducibility

The Fe_3O_4 -Au-IL/GCE operating at optimal Fe: Au mass ratio, deposition potential, and deposition time determined above, was applied to analyze 0 to 100 ppb of As (III) in 0.2 M pH 5 acetate buffer (Figure 7). The results show well-defined Gaussian shaped response with peak current around 0 V which increased with increasing As(III) concentration (Figure 7A). As illustrated in Figure 7B, the peak stripping current, i.e., response, was linearly related to As(III) concentration over the complete concentration range of 0 to 100 ppb. The sensitivity (the slope of the calibration plot) was 0.122 mA/ppb As(III) and the LOD (calculated based on $S/N = 3$) was 0.22 ppb. The high sensitivity and low LOD is credited to the combined effects of excellent absorption ability for As(III), high electrical conductivity and good stability of AuNPs, Fe_3O_4 NPs and IL. Table S2 shows a comparison of this work to the previous literature in terms of electrode material, technique, linear range, and limit of detection.

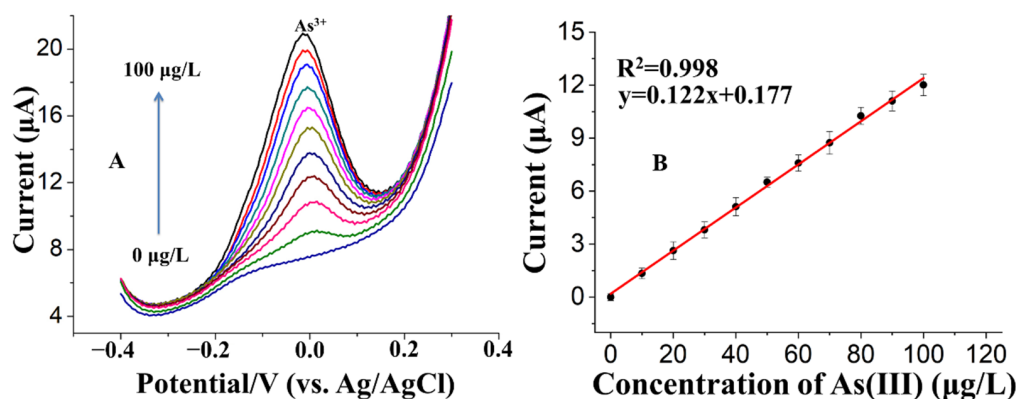


Figure 7. (A) SWAS voltammograms for additions of 0, 10, 20, 30, 40, 50, 60, 70, 80, 90 and 100 µg/L As(III). (B) The corresponding calibration curve of As(III).

Furthermore, the developed sensor demonstrated excellent reproducibility as evidenced by a very low (1.16%) relative standard deviation (RSD) for five repetitive measurements of 60 ppb As(III) (Figure S3).

3.4.2. Selectivity

Water sources contain a plethora of anions and cations that can potentially have a negative influence on the SWASV detection accuracy of As(III). We investigated the selectivity of the proposed sensor based on the analysis of 50 ppb of As(III) from 100-fold higher concentrations of Na^+ , K^+ , Ca^{2+} , Zn^{2+} , Mg^{2+} , Mn^{2+} and Fe^{2+} , and a 150-fold higher concentrations of Cl^- , NO_3^- , SO_4^{2-} , CO_3^{2-} , F^- and PO_4^{2-} . As shown in Figure 8, there were no measurable changes in the peak current signals (current variation $< \pm 10\%$) in the presence of all the tested ions, confirming the proposed $\text{Fe}_3\text{O}_4\text{-Au-IL/GCE}$ is efficient in the detection of As(III) in the presence of non-target species in water.

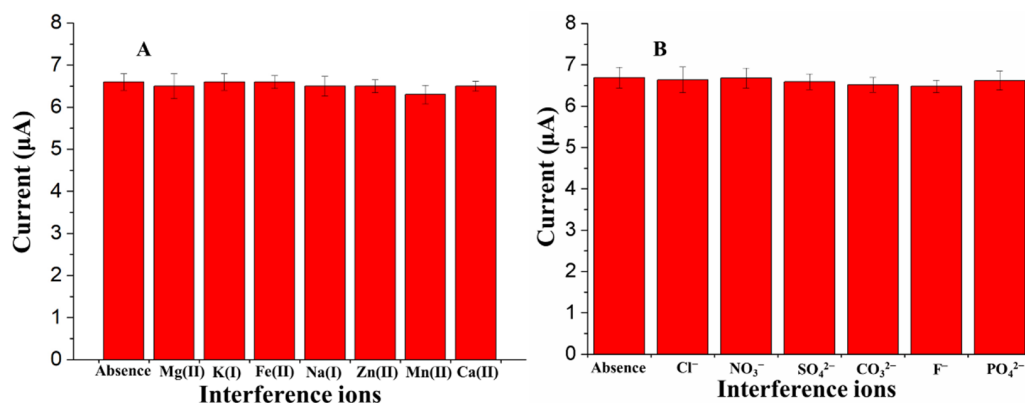


Figure 8. The selectivity of the proposed sensor in the presence of high concentrations of different ions (A: Cation; B: Anion) on the stripping peak current of 50 µg/L As(III) at $\text{Fe}_3\text{O}_4\text{-Au-IL/GCE}$ in 0.2 M acetate buffer (pH 5.0). Each data point is an average of 5 measurements from 3 electrodes and error bars represent ± 1 standard deviation.

3.5. Analysis of Simulated Water Samples

To evaluate the applicability of $\text{Fe}_3\text{O}_4\text{-Au-IL/GCE}$ for practical application, the sensor was applied to detect 5, 10 and 15 ppb of As(III) spiked in simulated river water representing the chemical composition of Yamuna River water in Northern India. Yamuna River is one of the most polluted rivers in India, and perhaps the world, with a complex matrix of pollutants [51,52]. As shown in Table 1, the recoveries (i.e., agreement) ranged from 97.2% to 101.3% (average of 99.06%) and the RSD ranged from 3.3% to 4.8% (average 3.9%). The excellent recoveries and low RSD demonstrate the promise of the developed

sensor for monitoring As(III) in real environmental samples. To further validate Fe₃O₄-Au-IL/GCE's robustness in complex wastewater streams, we used the sensor to detect As(III) in synthetic wastewater samples containing high concentrations of humic acid (50 mg/L), and compared it with values measured using ICP-MS. The Fe₃O₄-Au-IL/GCE sensor successfully determined As(III) concentrations, which were comparable to the results generated by ICP-MS (i.e., 95.4% ± 4.7%) indicating that Fe₃O₄-Au-IL/GCE is a robust electrode for detecting As(III) in complex water streams.

Table 1. Detection of As(III) in simulated river water.

Sample No.	Found ^a (µg/L)	Added (µg/L)	Detected after Adding ^a (µg/L)	Mean Recovery (%)	RSD (%)
1	3.12 ± 1.08	5	7.98 ± 1.23	97.2	4.8
2	4.89 ± 0.89	10	15.02 ± 1.15	101.3	3.3
3	9.95 ± 0.96	15	24.75 ± 0.90	98.67	3.6

^a Mean value ± Standard Deviation. Each data point is an average ± 1 standard deviation from 3 measurements using 3 electrodes.

4. Conclusions

In this work, an effective sensitive interface was designed using AuNPs decorated with Fe₃O₄NPs embedded in IL for the determination of As(III) at a trace level based on adsorbent-assisted in-situ electrocatalysis. The procedure for Fe₃O₄-Au synthesis introduced in this work (1) produced very tiny (≈10 nm) Fe₃O₄NPs enhancing the surface area for As(III) adsorption, (2) did not use a linker between gold and magnetite, which enhanced their combined effects, (3) is a green chemistry approach and (4) greatly reduced synthesis time (1–2 h). The proposed Fe₃O₄-Au-IL/GCE significantly enhanced the stripping response of As(III) as compared with the Fe₃O₄/GCE and AuNPs/GCE, as it provided a specific interface for As(III) to transfer electrons. Additionally, a Fe(II)/Fe(III) cycle and electrogenerated H₂ were activated to catalyze the reduction/stripping of the As(III)/As(0), which enabled a high sensitivity. The presence of IL in the composite contributed to better sensitivity and stability. The analytical, spectroscopic and microscopic features of the proposed Fe₃O₄-Au-IL/GCE characterization by XRD, EDX, TEM, SEM, EIS SWASV, and CV showed that the combined effect of AuNPs, Fe₃O₄ and IL resulted in a much better electrical conductivity, larger specific surface area and higher catalytic ability than the bare electrode. Moreover, several synthetic water samples were tested to further verify the practicability of the proposed platform. The results showed that Fe₃O₄-Au-IL/GCE can be successfully applied to the analysis of As(III) in synthetic river and wastewater samples without any sample pretreatment procedures, which suggested that it could be further applied to heavy metal analysis in real samples.

Supplementary Materials: The following are available online at <https://www.mdpi.com/1424-8220/21/3/883/s1>, Figure S1: EDX spectrum of the Fe₃O₄-Au nanocomposite, Figure S2: (A) Cyclic voltammograms and (B) Nyquist plot of electrochemical impedance spectra, Figure S3: Five repetitive stripping current measurements of 60 µg/L As(III) using the Fe₃O₄-Au-IL/GCE in 0.2 M acetate buffer, Table S1: The composition of synthetic raw wastewater, Table S2: Comparison of different electrodes for the detection of As(III).

Author Contributions: M.S. was responsible for materials synthesis and characterization, writing of the materials synthesis and characterization sections, original draft preparation and the revision of the manuscript; G.Z. was responsible for sensor fabrication, electrochemical measurements and original draft preparation; S.M. prepared the wastewater samples and interpreted the results; A.M. and D.J. conceptualized the project, acquired the funding, supervised the work, participated in design of the study and preparation of the original and revised manuscript. All authors have read and agreed to the published version of the manuscript.

Funding: This research was supported by the Department of Energy under award number FE0030456 and the DST/Intel[®]/Indo-U.S. Science and Technology Forum grant RP03472.

Institutional Review Board Statement: Not applicable.

Informed Consent Statement: Not applicable.

Data Availability Statement: Data sharing is not applicable to this article.

Acknowledgments: A.M. acknowledges the financial support of W. Ruel Johnson Chair. The authors acknowledge the use of ICP-MS core facility within the UC Center for Environmental Implications of Nanotechnology in CNSI at UCLA.

Conflicts of Interest: The authors have no conflicts of interest to declare.

References

1. Rodríguez-Lado, L.; Sun, G.; Berg, M.; Zhang, Q.; Xue, H.; Zheng, Q.; Johnson, C.A. Groundwater arsenic contamination throughout China. *Science* **2013**, *341*, 866–868. [[CrossRef](#)] [[PubMed](#)]
2. Smith, A.; Lopipero, P.; Chung, J.; Haque, R.; Hernandez, A.; Moore, L.; Steinmaus, C. Arsenic in drinking water and cancer risks estimated from epidemiological studies in Argentina, Chile, Taiwan and Japan. *Epidemiology* **2000**, *11*, S93.
3. Ning, Z.; Lobdell, D.T.; Kwok, R.K.; Liu, Z.; Zhang, S.; Ma, C.; Riediker, M.; Mumford, J.L. Residential exposure to drinking water arsenic in Inner Mongolia, China. *Toxicol. Appl. Pharmacol.* **2007**, *222*, 351–356. [[CrossRef](#)]
4. Feeney, R.; Kounaves, S.P. On-site analysis of arsenic in groundwater using a microfabricated gold ultramicroelectrode array. *Anal. Chem.* **2000**, *72*, 2222–2228. [[CrossRef](#)] [[PubMed](#)]
5. Tchounwou, P.B.; Patlolla, A.K.; Centeno, J.A. Invited reviews: Carcinogenic and systemic health effects associated with arsenic exposure—A critical review. *Toxicol. Pathol.* **2003**, *31*, 575–588. [[CrossRef](#)] [[PubMed](#)]
6. Shi, H.; Shi, X.; Liu, K.J. Oxidative mechanism of arsenic toxicity and carcinogenesis. *Mol. Cell. Biochem.* **2004**, *255*, 67–78. [[CrossRef](#)]
7. Melamed, D. Monitoring arsenic in the environment: A review of science and technologies with the potential for field measurements. *Anal. Chim. Acta* **2005**, *532*, 1–13. [[CrossRef](#)]
8. Rahman, M.R.; Okajima, T.; Ohsaka, T. Selective detection of As (III) at the Au (111)-like polycrystalline gold electrode. *Anal. Chem.* **2010**, *82*, 9169–9176. [[CrossRef](#)]
9. Mays, D.E.; Hussam, A. Voltammetric methods for determination and speciation of inorganic arsenic in the environment—A review. *Anal. Chim. Acta* **2009**, *646*, 6–16. [[CrossRef](#)]
10. Sengupta, M.K.; Sawalha, M.F.; Ohira, S.-I.; Idowu, A.D.; Dasgupta, P.K. Green analyzer for the measurement of total arsenic in drinking water: Electrochemical reduction of arsenate to arsine and gas phase chemiluminescence with ozone. *Anal. Chem.* **2010**, *82*, 3467–3473. [[CrossRef](#)]
11. Zaib, M.; Athar, M.M.; Saeed, A.; Farooq, U. Electrochemical determination of inorganic mercury and arsenic—A review. *Biosens. Bioelectron.* **2015**, *74*, 895–908. [[CrossRef](#)] [[PubMed](#)]
12. Cai, Y. Speciation and analysis of mercury, arsenic, and selenium by atomic fluorescence spectrometry. *TrAC Trends Anal. Chem.* **2000**, *19*, 62–66. [[CrossRef](#)]
13. Álvarez-Llamas, G.; del Rosario Fernández de la Campa, M.; Sanz-Medel, A. ICP-MS for specific detection in capillary electrophoresis. *TrAC Trends Anal. Chem.* **2005**, *24*, 28–36. [[CrossRef](#)]
14. Zhang, N.; Fu, N.; Fang, Z.; Feng, Y.; Ke, L. Simultaneous multi-channel hydride generation atomic fluorescence spectrometry determination of arsenic, bismuth, tellurium and selenium in tea leaves. *Food Chem.* **2011**, *124*, 1185–1188. [[CrossRef](#)]
15. Barek, J.; Peckova, K.; Vyskocil, V. Adsorptive stripping voltammetry of environmental carcinogens. *Curr. Anal. Chem.* **2008**, *4*, 242–249. [[CrossRef](#)]
16. Alves, G.M.S.; Magalhães, J.M.C.S.; Salaün, P.; Van den Berg, C.M.G.; Soares, H.M.V.M. Simultaneous electrochemical determination of arsenic, copper, lead and mercury in unpolluted fresh waters using a vibrating gold microwire electrode. *Anal. Chim. Acta* **2011**, *703*, 1–7. [[CrossRef](#)]
17. Castaneda, M.T.; Merkoçi, A.; Pumera, M.; Alegret, S. Electrochemical genosensors for biomedical applications based on gold nanoparticles. *Biosens. Bioelectron.* **2007**, *22*, 1961–1967. [[CrossRef](#)]
18. Martínez-Paredes, G.; González-García, M.B.; Costa-García, A. Lead sensor using gold nanostructured screen-printed carbon electrodes as transducers. *Electroanal. Int. J. Devoted Fundam. Pract. Asp. Electroanal.* **2009**, *21*, 925–930. [[CrossRef](#)]
19. Anker, J.N.; Hall, W.P.; Lyandres, O.; Shah, N.C.; Zhao, J.; Van Duyne, R.P. Biosensing with plasmonic nanosensors. *Nanoscience and technology: A collection of reviews from nature journals. World Sci.* **2010**, 308–319. [[CrossRef](#)]
20. Huang, J.; Chen, H. Heat-assisted electrodisolution of platinum in an ionic liquid. *Angew. Chem.* **2012**, *124*, 1716–1720. [[CrossRef](#)]
21. Sasaki, K.; Naohara, H.; Cai, Y.; Choi, Y.M.; Liu, P.; Vukmirovic, M.B.; Wang, J.X.; Adzic, R.R. Core-protected platinum monolayer shell high-stability electrocatalysts for fuel-cell cathodes. *Angew. Chem.* **2010**, *122*, 8784–8789. [[CrossRef](#)]
22. Guo, S.; Wang, E. Noble metal nanomaterials: Controllable synthesis and application in fuel cells and analytical sensors. *Nano Today* **2011**, *6*, 240–264. [[CrossRef](#)]
23. Bu, L.; Gu, T.; Ma, Y.; Chen, C.; Tan, Y.; Xie, Q.; Yao, S. Enhanced cathodic preconcentration of As (0) at Au and Pt electrodes for anodic stripping voltammetry analysis of As (III) and As (V). *J. Phys. Chem. C* **2015**, *119*, 11400–11409. [[CrossRef](#)]
24. Majid, E.; Hrapovic, S.; Liu, Y.; Male, K.B.; Luong, J.H.T. Electrochemical determination of arsenite using a gold nanoparticle modified glassy carbon electrode and flow analysis. *Anal. Chem.* **2006**, *78*, 762–769. [[CrossRef](#)]

25. Pungjunun, K.; Chaiyo, S.; Jantrahong, I.; Nantaphol, S.; Siangproh, W.; Chailapakul, O. Anodic stripping voltammetric determination of total arsenic using a gold nanoparticle-modified boron-doped diamond electrode on a paper-based device. *Microchim. Acta* **2018**, *185*, 324. [[CrossRef](#)]
26. Hokkanen, S.; Repo, E.; Lou, S.; Sillanpää, M. Removal of arsenic (V) by magnetic nanoparticle activated microfibrillated cellulose. *Chem. Eng. J.* **2015**, *260*, 886–894. [[CrossRef](#)]
27. Chandra, V.; Park, J.; Chun, Y.; Lee, J.W.; Hwang, I.-C.; Kim, K.S. Water-dispersible magnetite-reduced graphene oxide composites for arsenic removal. *ACS Nano* **2010**, *4*, 3979–3986. [[CrossRef](#)]
28. Xie, Z.; Xu, J.; Xie, F.; Xiong, S. Electrochemical detection of As (III) by a rGO/Fe₃O₄-modified screen-printed carbon electrode. *Anal. Sci.* **2016**, *32*, 1053–1058. [[CrossRef](#)]
29. Devi, P.; Sharma, C.; Kumar, P.; Kumar, M.; Bansod, B.K.S.; Nayak, M.K.; Singla, M.L. Selective electrochemical sensing for arsenite using rGO/Fe₃O₄ nanocomposites. *J. Hazard. Mater.* **2017**, *322*, 85–94. [[CrossRef](#)]
30. Wei, J.; Li, S.-S.; Guo, Z.; Chen, X.; Liu, J.-H.; Huang, X.-J. Adsorbent assisted in situ electrocatalysis: An ultra-sensitive detection of As (III) in water at Fe₃O₄ nanosphere densely decorated with Au nanoparticles. *Anal. Chem.* **2016**, *88*, 1154–1161. [[CrossRef](#)]
31. Li, S.-S.; Zhou, W.-Y.; Jiang, M.; Guo, Z.; Liu, J.-H.; Zhang, L.; Huang, X.-J. Surface Fe (II)/Fe (III) cycle promoted ultra-highly sensitive electrochemical sensing of arsenic (III) with dumbbell-like Au/Fe₃O₄ nanoparticles. *Anal. Chem.* **2018**, *90*, 4569–4577. [[CrossRef](#)] [[PubMed](#)]
32. Hassan, Y.; Chuang, C.-H.; Kobayashi, Y.; Coombs, N.; Gorantla, S.; Botton, G.A.; Winnik, M.A.; Burda, C.; Scholes, G.D. Synthesis and optical properties of linker-free TiO₂/CdSe nanorods. *J. Phys. Chem. C* **2014**, *118*, 3347–3358. [[CrossRef](#)]
33. Sedki, M.; Khalil, I.A.; El-Sherbiny, I.M. Hybrid nanocarrier system for guiding and augmenting simvastatin cytotoxic activity against prostate cancer. *Artif. Cells Nanomed. Biotechnol.* **2018**, *46*, S641–S650. [[CrossRef](#)] [[PubMed](#)]
34. Yoo, H.; Ahn, K.-H.; Lee, H.-J.; Lee, K.-H.; Kwak, Y.-J.; Song, K.-G. Nitrogen removal from synthetic wastewater by simultaneous nitrification and denitrification (SND) via nitrite in an intermittently-aerated reactor. *Water Res.* **1999**, *33*, 145–154. [[CrossRef](#)]
35. Wei, D.; Ivaska, A. Applications of ionic liquids in electrochemical sensors. *Anal. Chim. Acta* **2008**, *607*, 126–135. [[CrossRef](#)] [[PubMed](#)]
36. Pandey, S. Analytical applications of room-temperature ionic liquids: A review of recent efforts. *Anal. Chim. Acta* **2006**, *556*, 38–45. [[CrossRef](#)]
37. Rozniecka, E.; Shul, G.; Sirieix-Plenet, J.; Gaillon, L.; Opallo, M. Electroactive ceramic carbon electrode modified with ionic liquid. *Electrochem. Commun.* **2005**, *7*, 299–304. [[CrossRef](#)]
38. Khani, H.; Rofouei, M.K.; Arab, P.; Gupta, V.K.; Vafaei, Z. Multi-walled carbon nanotubes-ionic liquid-carbon paste electrode as a super selectivity sensor: Application to potentiometric monitoring of mercury ion (II). *J. Hazard. Mater.* **2010**, *183*, 402–409. [[CrossRef](#)]
39. Xiong, S.-Q.; Wei, Y.; Guo, Z.; Chen, X.; Wang, J.; Liu, J.-H.; Huang, X.-J. Toward membrane-free amperometric gas sensors: An ionic liquid–nanoparticle composite approach. *J. Phys. Chem. C* **2011**, *115*, 17471–17478. [[CrossRef](#)]
40. Huang, X.-J.; Aldous, L.; O'Mahony, A.M.; del Campo, F.J.; Compton, R.G. Toward membrane-free amperometric gas sensors: A microelectrode array approach. *Anal. Chem.* **2010**, *82*, 5238–5245. [[CrossRef](#)]
41. Das, R.S.; Singh, B.; Mukhopadhyay, S.; Banerjee, R. Gold nano particles catalyzed oxidation of hydrazine by a metallo-superoxide complex: Experimental evidences for surface activity of gold nano particles. *Dalt. Trans.* **2012**, *41*, 4641–4648. [[CrossRef](#)] [[PubMed](#)]
42. Olesiak-Banska, J.; Gordel, M.; Kolkowski, R.; Matczyszyn, K.; Samoc, M. Third-order nonlinear optical properties of colloidal gold nanorods. *J. Phys. Chem. C* **2012**, *116*, 13731–13737. [[CrossRef](#)]
43. Li, Y.; Yang, S.; Lu, X.; Duan, W.; Moriga, T. Synthesis and evaluation of the SERS effect of Fe₃O₄-Ag Janus composite materials for separable, highly sensitive substrates. *RSC Adv.* **2019**, *9*, 2877–2884. [[CrossRef](#)]
44. Márquez, F.; Herrera, G.M.; Campo, T.; Cotto, M.; Ducongé, J.; Sanz, J.M.; Elizalde, E.; Perales, Ó.; Morant, C. Preparation of hollow magnetite microspheres and their applications as drugs carriers. *Nanoscale Res. Lett.* **2012**, *7*, 210. [[CrossRef](#)] [[PubMed](#)]
45. Krishnamurthy, S.; Esterle, A.; Sharma, N.C.; Sahi, S. V Yucca-derived synthesis of gold nanomaterial and their catalytic potential. *Nanoscale Res. Lett.* **2014**, *9*, 627. [[CrossRef](#)] [[PubMed](#)]
46. Van Quy, D.; Hieu, N.M.; Tra, P.T.; Nam, N.H.; Hai, N.H.; Thai Son, N.; Nghia, P.T.; Van Anh, N.T.; Hong, T.T.; Luong, N.H. Synthesis of silica-coated magnetic nanoparticles and application in the detection of pathogenic viruses. *J. Nanomater.* **2013**, *2013*. [[CrossRef](#)]
47. Adams, D.M.; Brus, L.; Chidsey, C.E.D.; Creager, S.; Creutz, C.; Kagan, C.R.; Kamat, P.V.; Lieberman, M.; Lindsay, S.; Marcus, R.A. Charge transfer on the nanoscale: Current status. *J. Phys. Chem. B* **2003**, *107*, 6668–6697. [[CrossRef](#)]
48. Sedki, M.; Chen, X.; Chen, C.; Ge, X.; Mulchandani, A. Non-lytic M13 phage-based highly sensitive impedimetric cytosensor for detection of coliforms. *Biosens. Bioelectron.* **2020**, *148*, 111794. [[CrossRef](#)]
49. Zhao, G.; Sedki, M.; Ma, S.; Villarreal, C.; Mulchandani, A.; Jassby, D. Bismuth subcarbonate decorated reduced graphene oxide nanocomposite for the sensitive stripping voltammetry analysis of Pb(II) and Cd(II) in water. *Sensors* **2020**, *20*, 6085. [[CrossRef](#)]
50. Renock, D.; Voorhis, J. Electrochemical investigation of arsenic redox processes on pyrite. *Environ. Sci. Technol.* **2017**, *51*, 3733–3741. [[CrossRef](#)]
51. Misra, A.K. A river about to die: Yamuna. *J. Water Resour. Prot.* **2010**, *2*, 489. [[CrossRef](#)]
52. Malik, D.; Singh, S.; Thakur, J.; Singh, R.K.; Kaur, A.; Nijhawan, S. Heavy metal pollution of the Yamuna River: An introspection. *Int. J. Curr. Microbiol. Appl. Sci.* **2014**, *3*, 856–863.